ACS ES&T Water

pubs.acs.org/estwater

Article

Field and Laboratory Evidence for Manganese Redox Cycling Controlling Iron and Arsenic Retention in Household Sand Filters

Anh Van Le,* E. Marie Muehe, Sharon Bone, Sören Drabesch, Stefan Fischer, and Andreas Kappler*

Cite This: *ACS EST Water* 2024, 4, 33−43

Read Online

ACCESS | Metrics & More | Article Recommendations | Supporting Information

ABSTRACT: Application of household sand filters (SFs) is widespread in low-income regions, such as West Bengal, Bangladesh, and Vietnam, for the removal of groundwater contaminants including Fe, Mn, and As. SF operation typically transitions from (oxic) unsaturated conditions to saturated conditions, creating oxygen-limited zones within sand layers. To ensure the safe and effective use of SFs, understanding filter performance and spatiotemporal changes of solid-associated Fe, As, and Mn in different saturation conditions is crucial but remains unknown. Therefore, column experiments were conducted to follow Fe, As, and Mn removal and their distribution and speciation on sand grain surfaces under unsaturated and saturated conditions. On average, 99 ± 0.2, 93 ± 0.7, and 91 ± 8% of $Fe(II)_{aq}$, $As(III)_{aq}$, and $Mn(II)_{aq}$ were removed under unsaturated conditions. Under saturated conditions, Fe and As removal remained constant, whereas up to 5 mg/L $Mn(II)_{aq}$ was leached from columns. μXANES analysis showed that solid-associated Fe(III), As(V), and Mn(III)/(IV) dominated in unsaturated sand. However, under saturated conditions, up to 46 and 15% of Fe(III) and As(V) were reduced, and the presence of Mn(II) was confirmed in the anoxic zones. The results suggest that Mn(IV) oxides formed during unsaturated conditions, serving as hosts and oxidants for Fe and As in SFs under reducing conditions.

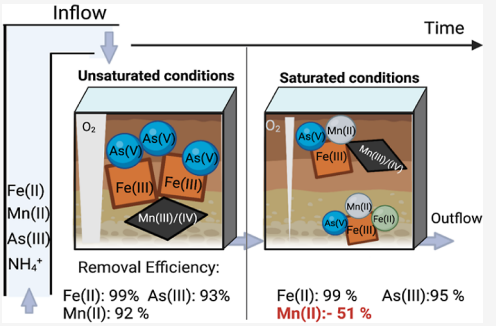

KEYWORDS: *sand filters, biogeochemical processes, Fe, Mn, As*

1. INTRODUCTION

Water filtration by household sand filters (SFs) is one the oldest point-of-use water treatment techniques that has been recommended by the World Health Organization (WHO) to provide safe drinking water for people living in rural areas.[1,2] In the Red River delta, Vietnam, groundwater is acutely contaminated by As; up to 3000 μg/L of As was detected in some places.[3] Household SFs have been used in this area to eliminate As(III) and other contaminants such as Fe(II) and Mn(II) from groundwater for more than 30 years.[4,5] Groundwater is pumped intermittently onto the top of the sand surface, followed by gravitational trickling through the sand layer. Filtered water is collected in a lower compartment for cleaning and drinking.[5,6] As(III), Fe(II), and Mn(II) are co-oxidized in the filter, followed by the precipitation of As(V)-bearing Fe(III) (oxyhydr)oxides and Mn(III/IV) oxides on sand particle surfaces.[7,8]

The operation of the SF starts with unsaturated flow when sand layers maintain oxic conditions and is followed by saturated flow when an oxygen gradient is formed along the sand column creating semioxic (top layer) and anoxic zones (bottom layer). When the filters become clogged (every 3−6 months), 10−20 cm of the top sand is scraped off for unclogging. Thus, SFs have usually been operated under alternating unsaturated and saturated flow for many years.

Under unsaturated conditions, Fe, Mn, and As species in the groundwater are completely oxidized (Fe(III), Mn(IV), and As(V)). Mn oxides are therefore constantly formed in SFs, leading to distinguished black patches or layers in the filters.[6,9] The formation of Mn(IV) oxides is due to (i) microbial activity of Mn(II)-oxidizing bacteria (MnOB)[10,11] and (ii) abiotic oxidation of Mn(II) by O_2 catalyzed at Fe(III) (oxyhydr)oxide mineral surfaces.[12−14] Since Mn(IV) oxides are strong oxidants, they can directly oxidize dissolved As(III) and Fe(II) in the groundwater (eqs 1 and 2).

$$MnO_2 + AsO_3^{3-} + 2H^+ \rightarrow Mn^{2+} + AsO_4^{3-} + H_2O \quad (1)$$

$$2MnO_2 + Fe^{2+} + 5H^+ \rightarrow Fe(OH)_3 + 2Mn^{2+} + H_2O \quad (2)$$

Over a long operational time (several months to years), the filter surface gets blocked by precipitation of carbonate minerals and metal (oxyhydr)oxides, thus inhibiting the abiotic

Received: May 10, 2023
Revised: September 20, 2023
Accepted: September 21, 2023
Published: October 4, 2023

oxidation of Fe(II) and As(III) by O_2.[15] Under such conditions, Mn oxides might complement the heterogeneous oxidation of As(III) and Fe(II) by O_2 (eqs 1 and 2) to enhance As and Fe retention in SFs. Indeed, under O_2-depleted conditions, Mn(IV) oxides (either as abiotic or biogenic birnessite) prevented As mobilization in soil and sand columns.[16−18] However, until now, there is no direct evidence that under O_2-depleted conditions the presence of Mn(IV) oxides can control the immobilization of As and Fe in household SFs. One of the issues is that most studies have examined As, Fe, and Mn removal by sampling at specific time points to confirm the high removal efficiency. There are inadequate data regarding long-time monitoring of Fe, As, and Mn effluent over unsaturated (fully oxic) to saturated (O_2-depleted) operational phases in SFs. Obtaining such analyses at different time points (with different saturation status and different redox conditions) is essential as it will reveal whether As removal mechanisms change during redox fluctuations and can reveal the impact of Mn(III/IV) oxides on As and Fe retention in SFs.

Therefore, in this study, a series of column experiments were conducted in the laboratory and in the field in which sand columns were fed by sterile artificial and local native groundwater, respectively. We aimed at (i) monitoring the performance of the SF applied to remove As, Fe, and Mn over time from unsaturated to saturated conditions, (ii) quantifying the distribution of total As, Fe, and Mn along the depth of sand columns, and (iii) identifying the location and speciation of As, Fe, and Mn on the surface of sand particles under unsaturated and saturated conditions.

2. MATERIALS AND METHODS

2.1. Column Setup. The glass columns (inner diameter 4.5 cm, length 25 cm) consisted of support layers filled with 2 cm of gravel (particles size 6−8 mm, Flairstone, Germany) and 3 cm sterilized quartz sand (particle size 0.4−0.8 mm, Carl Roth GmbH, Germany) at the bottom, followed by a reactive layer filled with 10 cm of SF materials. Columns were intermittently operated in gravitational downflow mode 2−3 times per day. Two similar column setups were running in the field (20°55′08.63″ N, 105°53′47.61″ E, Van Phuc village in the Red River delta, Vietnam) (field site description see Supporting Information, Section S1) and in the lab.

2.2. Column Flow Experiment. *2.2.1. Columns in the Field.* In the field, the biotic columns contained the reactive layer (top 10 cm) filled with sand collected from the local sand supplier. 250 mL of natural groundwater was pumped directly on top of the sand columns each time. The inflow water contained 16.1 mg/L Fe(II), 1.4 mg/L Mn(II), and 240 μg/L of As(III). The filtration rate and the concentrations of Fe, Mn, and As in the effluent were recorded at every feeding batch. The experiment ran over 1.5 months, equaling 169 pore volumes under temperatures ranging from 20 to 25 °C.

2.2.2. Columns in the Laboratory. In the laboratory, the duplicate biotic columns contained a reactive layer (top 10 cm) filled with sand collected from a frequently running household filter at the same location as the field experiment (sample collection is described in Supporting Information, Section S1). Additionally, an abiotic control column was set up in the lab, with the reactive layer (top 10 cm) filled with sterile quartz sand (particle size: 0.4−0.8 mm, Carl Roth GmbH, Germany). To follow the dissolved oxygen (DO) in the sand columns (biotic and abiotic setups), six pieces of oxygen optode foil (PreSens, Germany) were glued at different depths along the columns. Sterile artificial groundwater (AGW) was freshly prepared every week and contained 20.9 ± 1.5 mg/L of Fe(II), 1.8 ± 0.6 mg/L of Mn(II), and 307.0 ± 24.4 μg/L of As(III). The preparation of AGW is described in Supporting Information Section S2 and Table S1. The pH of AGW was adjusted to 7.3 which is the average pH value of groundwater in the Red River delta.[5] Every time, up to 150 mL of ARW was fed to the columns. In total, the experiment was operated over two months equaling 141 pore volumes, and the columns experienced two clogging events at pore volumes 93 and 141. After the first clogging event, 3 cm of top sand was scraped off the column to unclog the sand column, and the experiment was continuously running until the second clogging. The column experiments in the laboratory were performed at a temperature ranging from 20 to 25 °C similar conditions as the field experiment.

2.3. Aqueous Analysis. At every filtration time, inflow and outflow water was collected. To quantify dissolved As, Fe, and Mn, 2 mL of inflow and outflow water were filtered (0.22 μm cellulose filter, EMD Millipore) and diluted with 1% HNO_3 before analysis by inductively coupled plasma mass spectrometry (ICP−MS) (Agilent 7900, Agilent Technologies).

2.4. Solid Phase Analysis. After the experiments, to prevent further oxidation of solid-associated Fe(II), As(III), and Mn(II), filter materials were collected from 2 to 5 cm depth in the glovebox (100% N_2, <30 ppm of O_2, MBRAUN UNIlab). Samples were stored anoxically in 100 mL Schott bottles in the freezer (−20 °C) until further analysis.

2.4.1. Elemental Composition Analysis. Twelve mL portion of aqua-regia solution (9 mL of 37% HCl and 3 mL of 65% HNO_3) was added slowly to the Xpress Plus Teflon vessels containing 0.5 g of dried sand materials. The samples were digested in the Microwave Accelerated Reaction System, MARS 6 (CEM, USA) (details in Supporting Information Section S3). Afterward, the digested samples were adjusted to a final volume of 50 mL by adding Milli-Q H_2O under the fume hood. The samples were centrifuged at 16,873*g* for 15 min (Thermo Scientific Sorvall LYNX6000). 100 μL aliquot of the supernatant was collected and diluted 100-fold in 1% HNO_3. Samples were stored at 4 °C in the dark until analysis via the Agilent 7900 ICP−MS.

2.4.2. X-ray Fluorescence Imaging. The distribution of As, Fe, and Mn on the surface of sand particles was visualized using X-ray fluorescence (XRF) mapping using beamline 7-2 at the Stanford Synchrotron Radiation Lightsource (SSRL). Samples were freeze-dried and transferred to wells with 5 mm diameter on multiwell sample holders. Samples were embedded in an Epotek 301-1 resin (Epoxy Technology). All preparatory steps were performed in a glovebox (100% N_2, <30 ppm of O_2). Epoxied samples were polished to a 5 mm thickness under oxic (ambient) conditions.

Beamline 7-2 is equipped with a bend magnet, capillary optics, and a double-crystal (Si 111) monochromator. Samples were placed 45° to the incoming focused beam with a 50 μm spot size and a 100 ms dwell time per pixel. Samples were imaged at two energies, 12,000 eV for obtaining As and total elemental maps and 8000 eV for obtaining accurate Fe and Mn maps. Fluorescence intensities of selected elements were monitored using a four-element Vortex Silicon Drift Detector.

As, Fe, and Mn maps were visualized in SMAK[19] with details in Supporting Information Section S4. Locations with a simultaneous presence of high counts of As, Fe, and Mn were

https://doi.org/10.1021/acsestwater.3c00245
ACS EST Water 2024, 4, 33−43

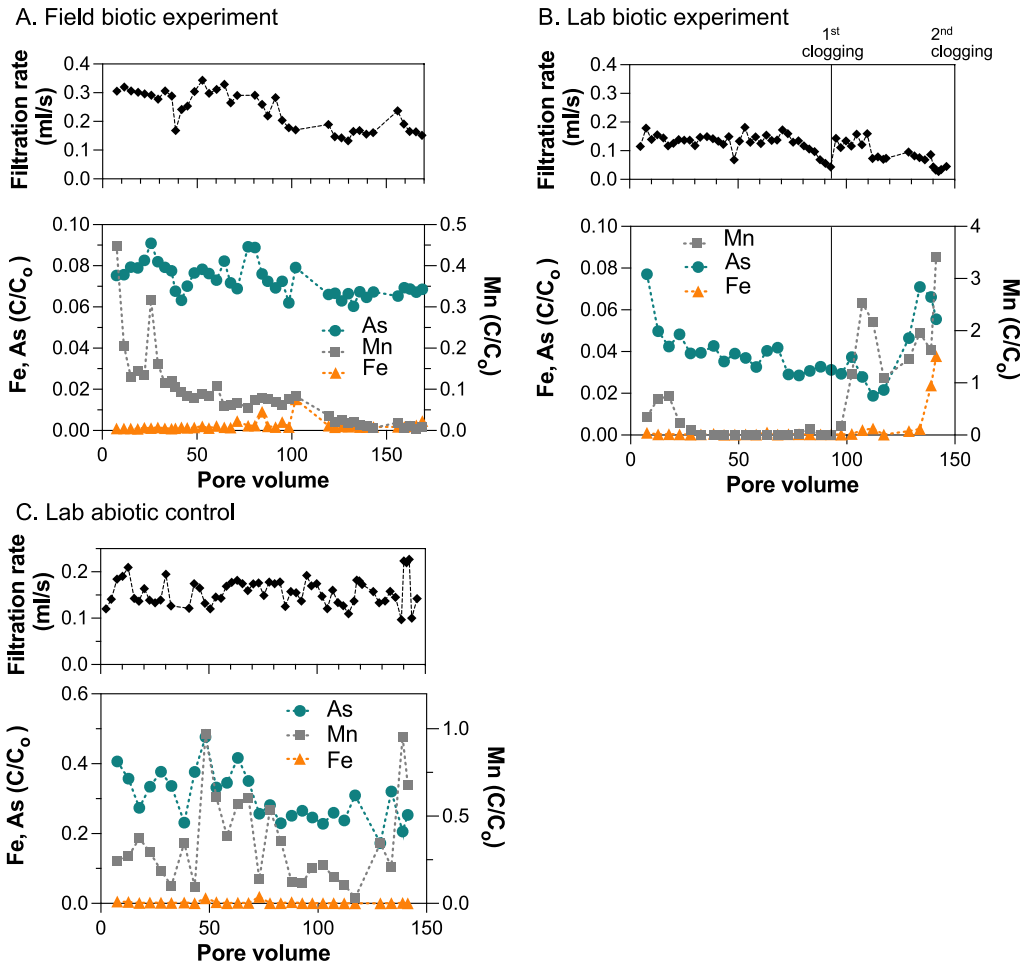

Figure 1. Filtration rate (upper panel) and relative effluent concentration (C/C_0, where C and C_0 are effluent and influent concentration, respectively) of Fe, Mn, and As (lower panel) in the field-based biotic setups (A), lab-based biotic setups (B) and the abiotic control (C). The filtration rate as well as the concentrations of Fe, Mn, and As in the influent and effluent were recorded at every feeding batch.

identified and selected for μ-X-ray absorption near edge structure (μ-XANES) spectroscopy. Mn K-edge, Fe K-edge, and last As K-edge μXANES data were obtained in this order at the same locations (50 μm spot), starting with the lowest energy to prevent beam redox changes. Three to six spectra were obtained per spot, depending on spectra quality. The spectra were processed in Athena[20] with details in Supporting Information Section S5.

2.4.3. Scanning Electron Microscopy. The morphology of precipitates coated on the sand particles' surface was analyzed by scanning electron microscopy (SEM) using a Zeiss Crossbeam 550L Scanning Electron Microscope (Zeiss, Germany). Filter materials collected from saturated and unsaturated columns were dried in an oven at 30 °C and then placed on aluminum SEM sample holders onto carbon adhesive tabs. The samples were sputter-coated with 8 nm of platinum with a BALTEC SCD 500 sputter coater. SEM micrographs were collected using the secondary electron secondary ion detector with an accelerating voltage of 5 kV.

3. RESULTS AND DISCUSSION

3.1. Long-Term Monitoring of As, Mn, and Fe in the Effluent. *3.1.1. Field Column Experiment.* Column experiments in the field were performed over 169 pore volumes in 1.5 months under unsaturated conditions (flow rate ranged from 0.3 to 0.15 mL/s) (Figure 1A). The columns were fed twice per day by natural groundwater containing 16.1 mg/L Fe(II), 1.4 mg/L Mn(II), and 240 μg/L As(III) (Table S2). Low concentrations of Fe, Mn, and As in the outflow indicated high and stable removal efficiencies by the SFs. The relative effluent values (C/C_0, where C and C_0 are effluent and influent concentration, respectively) for Fe, Mn, and As were 0.002, 0.08, and 0.07 (Figure 1) which corresponded to effluent concentrations of 38, 117, and 17.5 μg/L, respectively (Figure S3). The residual As concentration in the water after filtration was higher than that in the WHO drinking water standard (10 μg/L). Our observation is consistent with other studies investigating full-scale household filters in the Red River delta,[6,7,9] suggesting that further As treatment steps are required for drinking purposes.

3.1.2. Laboratory Column Experiment. To further investigate the effect of saturated versus unsaturated conditions on the filter performance, we conducted a similar column experiment in the lab. The aim of the laboratory experiment was to investigate the filter performance under saturated conditions. Therefore, a slower flow regime than in the field experiment was selected, starting from 0.14 mL/s (the flow rate in the field ranged from 0.3 to 0.15 mL/s) (Figure 1A). The abiotic control was performed with sterile quartz sand added to the column instead of native sand materials collected from household filters in Vietnam. Both abiotic and biotic setups were fed by sterile, anoxic, AGW containing 20.9 ± 1.5

https://doi.org/10.1021/acsestwater.3c00245
ACS EST Water 2024, 4, 33−43

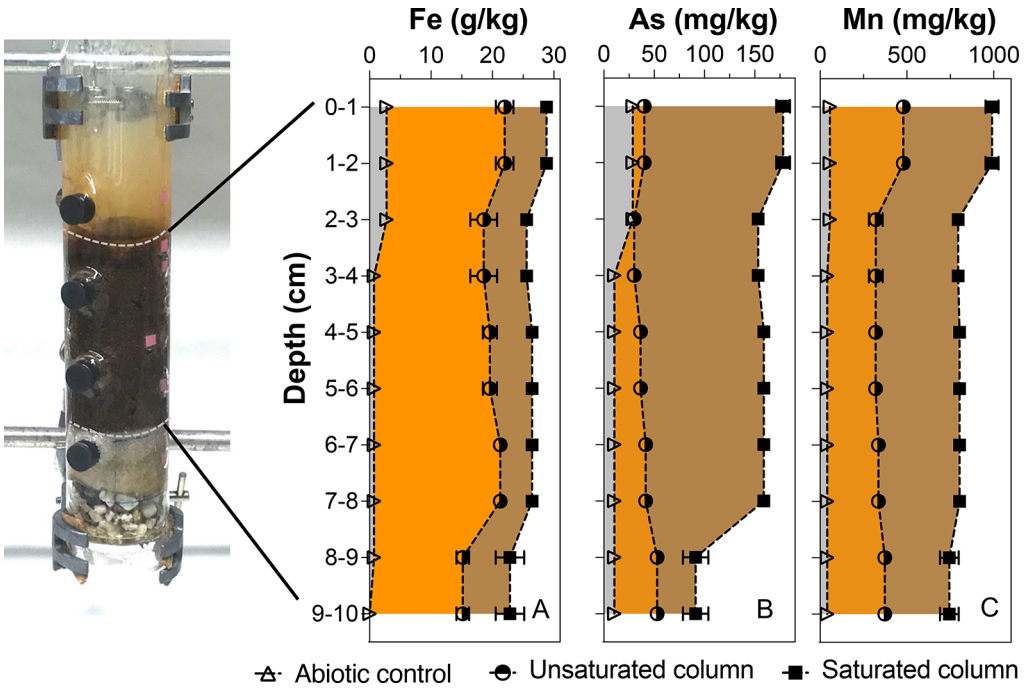

Figure 2. Vertical distribution of Fe (A), As (B), and Mn (C) in abiotic control (black), unsaturated (orange), and saturated (brown) columns. All samples were analyzed in triplicate, and error bars indicate the standard deviation.

mg/L of Fe(II), 1.8 ± 0.6 mg/L of Mn(II), and 307.0 ± 24.4 μg/L of As(III) (Table S2).

The performance of the biotic sand column was divided into two phases (Figure 1B). In the first phase (93 pore volumes, before the first clogging), the sand column remained oxic with a DO in the porewater ranging between 4 and 6 ppm (Figure S4). Fe, Mn, and As were effectively removed with relative effluent concentrations (C/C_0) of 0.0004, 0.13, and 0.04, respectively (Figure 1B). We noticed that the Fe and As removal efficiency in the laboratory setup was higher than in the field, probably due to the absence of Si and higher Ca in the AGW relative to natural groundwater. Silicate has a weaker adsorption affinity to Fe(III) (oxyhydr)oxides compared to As(III) and As(V);[21] therefore, Si is only a weak competitor of As regarding adsorption on Fe(III) phases during filtration. In contrast, Ca was shown to enhance As retention by forming Ca−As(V) bonds on the sand particle surface.[22,23]

During the second phase between the first and second clogging (pore volumes 93−141), the column was operated under semioxic conditions (DO of porewater < 0.5 ppm) (Figure S4). After the first clogging, 3 cm of the top sand was scraped off; then, the column was continuously run until the second clogging event. Fe removal efficiency was comparable to phase 1 ($C/C_{0(Fe)}$: 0.009), while Mn breakthrough occurred throughout this phase as the Mn concentration in the effluent was constantly higher than in the influent with C/C_0 ranging between 1 and 3.5 (Figure 1B). Arsenic removal slightly changed from 8.9 to 12.6 μg/L in the effluent (Figure S3). The drop in the DO along the sand column in the second phase compared with the first phase suggests the formation of anoxic zones along the sand column. Under such conditions, it might lead to a reduction of As-bearing Fe(III) (oxyhydr)oxides forming As(III) and Fe(II). Therefore, MnO_2 could be involved in the oxidation of reduced As(III) and Fe(II) to varying extents (Ep 1, 2). This explained an increase in mobile Mn(II) at the effluent and the high retention of Fe and As in the sand column. In the abiotic control column, 99% of the Fe(II) was removed by abiotic oxidation with O_2, but As and Mn removal was limited to 70 and 66%, respectively (Figure 1C). These findings clearly show the important roles of microbial oxidation of Fe(II), As(III), and Mn(II) in order to complement the abiotic processes to maintain high removal rates of Fe, As, and Fe in the sand column as shown before by Van Le et al.[9]

3.2. Distribution of Solid Fe, As, and Mn in Unsaturated and Saturated Columns. To understand changes in Fe, As, and Mn distribution in different depth layers in the unsaturated column (field setup) and saturated column (laboratory setup), total Fe, As, and Mn associated with sand materials at every 2−5 cm depth were analyzed by ICP−MS after microwave digestion.

Fe, As, and Mn accumulated in the top 2−3 cm of the sand columns, and their concentrations decreased with filter depth. Since the groundwater in the Red River delta is enriched with Fe(II), Fe showed the highest abundance in the sand column. Up to 18.5−22.0 and 26.5−28.8 g/kg were found in unsaturated and saturated columns, respectively (Figure 2A). Manganese in the solid phase of the saturated sand column was between 744 and 991 mg/kg, twice as much as in the unsaturated column (Figure 2B). Arsenic was enriched in the saturated column with a concentration between 159 and 178 mg/kg, which was three times as high as that for As in the unsaturated column (Figure 2C). Since the removal efficiency of the abiotic columns was lower than in the biotic ones, the Fe, As, and Mn retained in the sand was up to 10 times less than in the biotic setups.

At the macro scale, both As and Mn linearly correlated with Fe with correlation factors R^2 from 0.82 to 0.99 in both unsaturated and saturated columns (Figures S5 and S6), suggesting that As adsorbed on Fe(III) (oxyhydr)oxides on the sand particles as reported before.[6,7] In contrast, As and Mn were less colocated indicated by lower correlation factors,

https://doi.org/10.1021/acsestwater.3c00245
ACS EST Water 2024, 4, 33−43

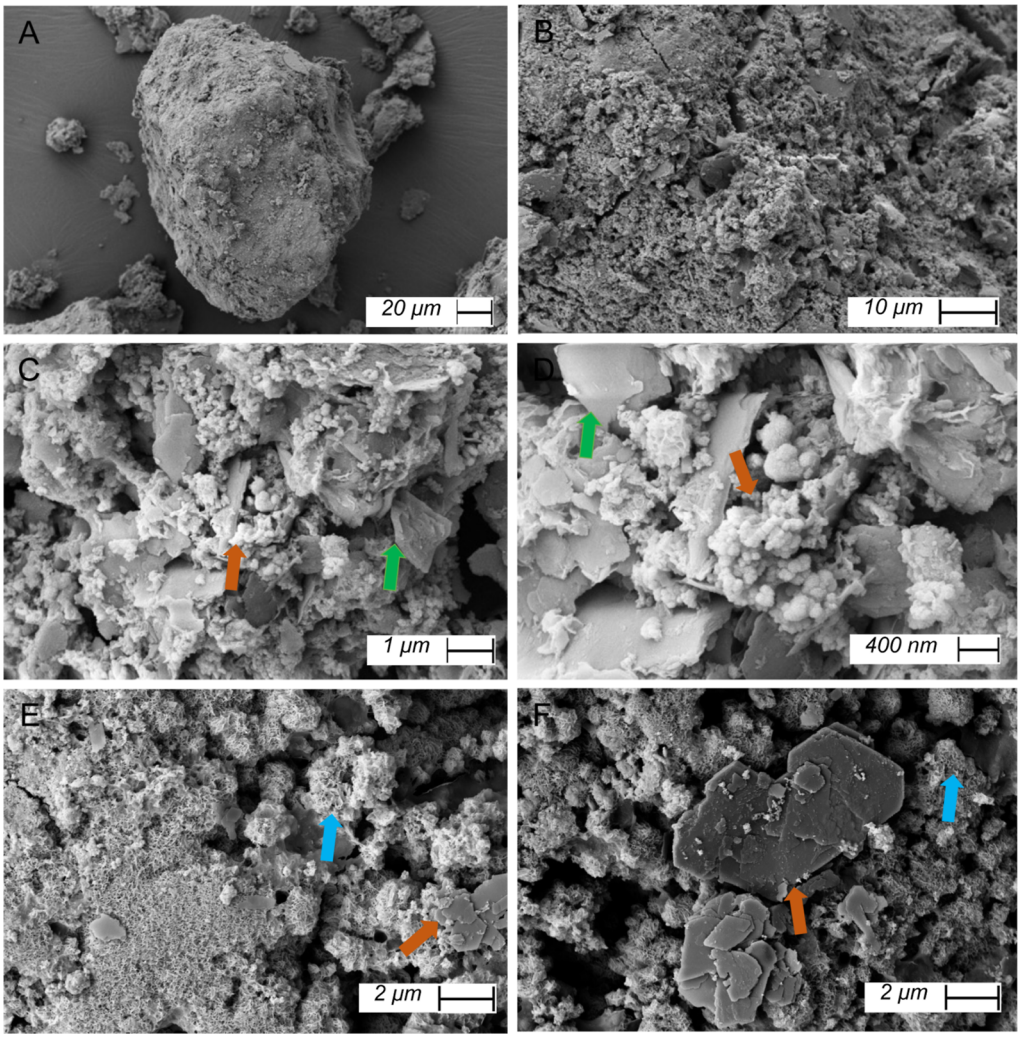

Figure 3. Scanning electron micrographs showing the distribution of precipitates on the sand particle surface (A,B). The most dominant mineral structures were microplatelets (green arrows) associated with nanoglobular aggregates (orange arrows) (C,D) and nanoflower shapes (blue arrows) (E,F).

which were 0.55 and 0.8 for unsaturated and saturated columns, respectively. The element distributions in unsaturated and saturated columns followed the same pattern. Thus, we hypothesize that the changes in Fe, As, and Mn concentrations might occur due to changes in speciation and the binding environment. It must be noted that new sand material was used for the field experiment (unsaturated conditions). In contrast, sand material collected from existing household filters was used for the laboratory experiment (saturated conditions) to evaluate the microbial activities in the sand. Therefore, filter materials in the saturated column already contained higher amounts of Fe, As, and Mn than the unsaturated column, which could lead to catalytic effects.[8,24]

3.3. Morphology of Precipitates and Elemental Distribution on Sand Particle Surface. SEM and μXRF were combined to assess the sand particle size (Figure 3A and S7), the morphology of minerals (Figure 3B−D), and the elemental distribution on the sand particle surfaces (Figure 4, S8, and S9). The results indicated a heterogeneous elemental distribution and micro- to nanosized mineral structures coating sand particle surfaces. Three mineral structures were identified including microplatelets associated with nanoglobular aggregates (Figure 3C,D) and nanoflower-shaped structures (Figure 3E,F). The nanoglobules had a similar structure to Fe nanoaggregates found on the surface of sand particles in other Fe−Mn-based sand filtration systems.[25,26] We suggest that the flower-like nano morphology is similar to the birnessite structure reported in previous studies.[26,27] The identified mineral structures could originate from the filter materials or were newly formed during filtration. Further SEM imaging of the local raw sand materials should be included in future studies to better distinguish the origins of these precipitates.

Pixel fluorescence counts of Fe, As, and Mn collected from μXRF maps indicated a stronger correlation of Fe and Mn (R^2 = 0.5−0.6) than that of Fe and As (R^2 = 0.2−0.4) in both unsaturated and saturated columns. However, in selected areas, both As and Mn were strongly correlated with Fe with $R^2 > 0.8$ (Figure 4E,F, S8, and S9), while the correlation factor of Mn and As was lower ($R^2 < 0.7$) (Figure 4F). The Fe, As, and Mn correlations at the micro-scale were in line with the findings at the macro scale. Additionally, Mn was associated with Fe(III) (oxyhydr)oxides in the unsaturated sample (R^2 = 0.73) (Figure S8), while in the saturated sample, Fe−Mn-rich areas were detected in fewer locations indicated by a lower correlation factor (R^2 = 0.6) (Figure 4B). Arsenic possessed a lower

https://doi.org/10.1021/acsestwater.3c00245
ACS EST Water 2024, 4, 33−43

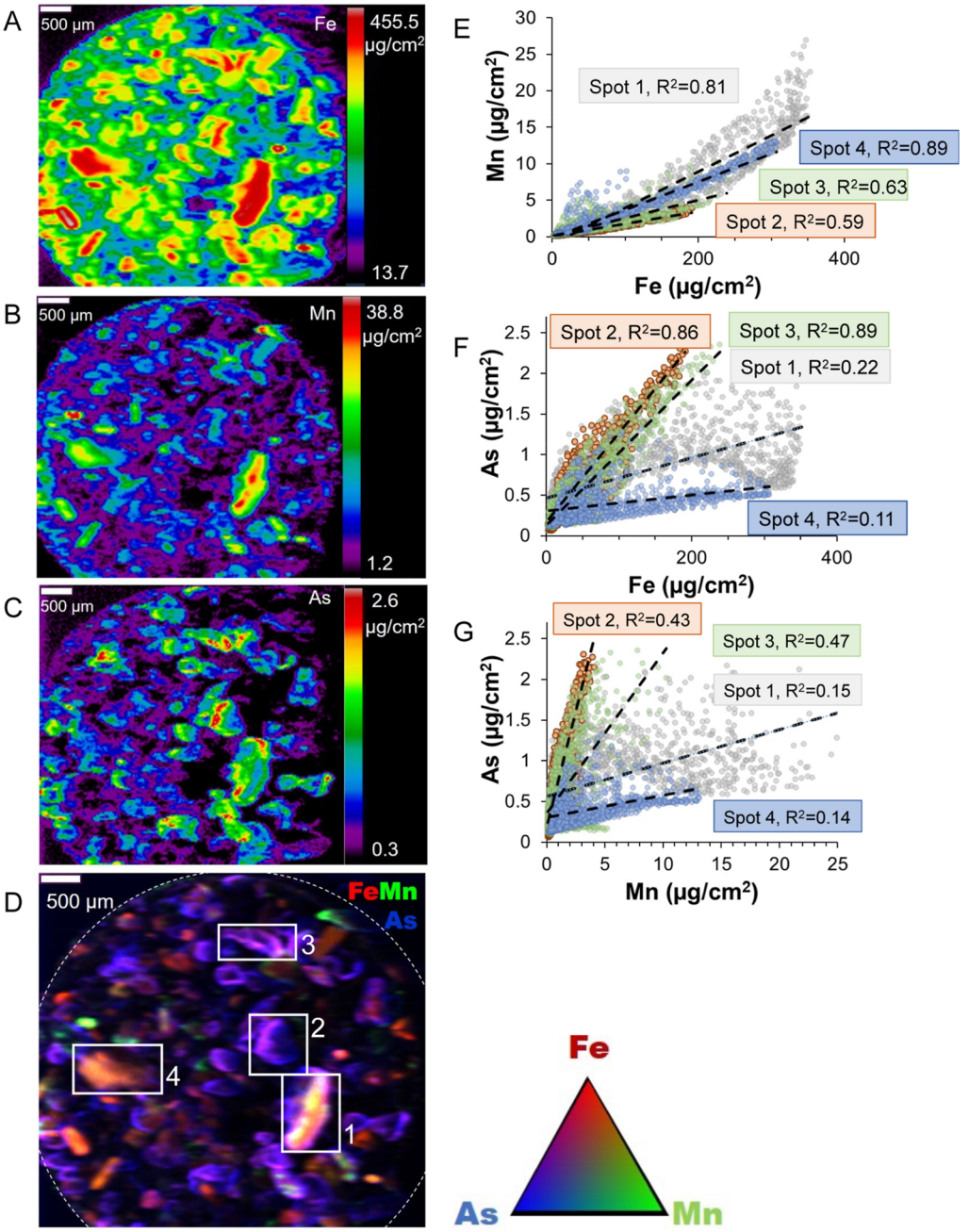

Figure 4. Multiple energy μ-XRF maps of SF materials from saturated columns operated in the lab. μ-XRF maps of Fe (A), Mn (B), and As (C) distributed on sand surfaces and their tricolor map (D). Correlations of Mn vs Fe (E), As vs Fe (F), As vs Mn (G), and their correlation coefficient (R^2) were displayed for 4 selected areas from tricolor map.

concentration than Mn and Fe and enriched as rims at the mineral's surface water (solid−water) interface (Figure 4C) that is also described in previous studies.[7,28,29]

Additionally, other elements such as P, Ca, and Si also showed strong partitioning into the Fe(III) (oxyhydr)oxide phase (Figure S10), probably influencing As removal in SFs. Iron was well colocated with P in all samples as phosphate is preferentially adsorbed to Fe(III) (oxyhydr)oxide compared to As(V), As(III), and silicate.[21,30] Thus, low Fe/P ratios (0.05−1) of the groundwater were an asset for high As retention. Tricolor maps of Si, Ca, and Fe indicated a lower amount of Si and Ca associated with Fe (Figure S10). Most detected Si fluorescence counts stemmed from the sample holder (made from quartz). Ca-rich sand crusts were found separately from the Fe signal, probably precipitated as calcite in the filters.

3.4. Fe, As, and Mn Speciation in Saturated and Unsaturated Sand Columns. Filter materials were collected from different depth layers (2−5 cm) in unsaturated and saturated columns. Redox states of Mn, Fe, and As on selected areas from μXRF maps were analyzed by μXANES spectroscopy using linear combination fitting (LCF) (Figure 5A−C). μXANES spectra of different areas on the same sample were almost identical, indicating that the speciation distribution was homogeneous and representative of that sample. The proportions of Fe(II) and As(III) in each sample were converted to concentrations for a better quantitative comparison between unsaturated and saturated columns

https://doi.org/10.1021/acsestwater.3c00245
ACS EST Water 2024, 4, 33−43

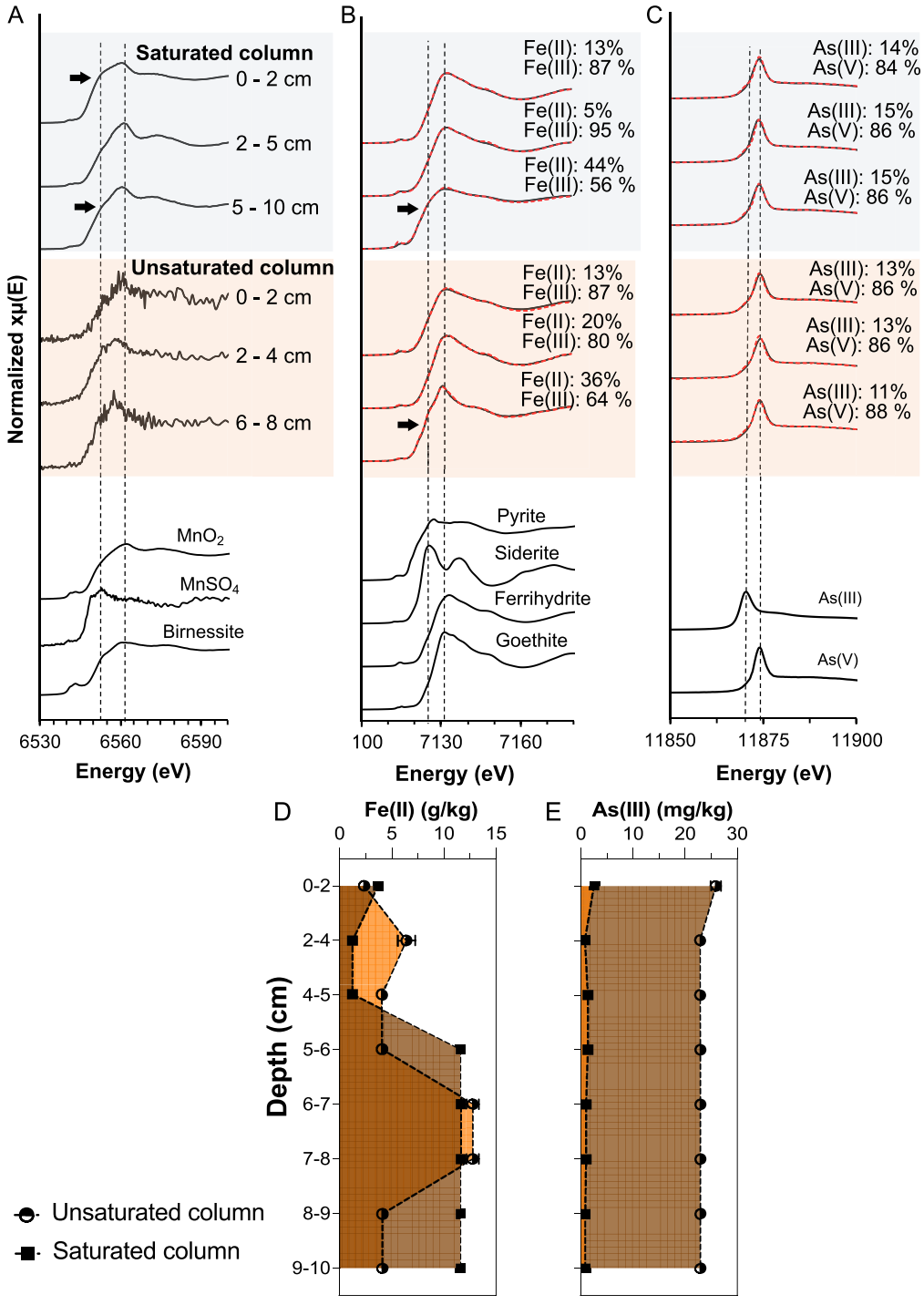

Figure 5. Normalized K-edge μXANES spectra of Mn (A), Fe (B), and As (C) in filter materials at different depths in the saturated and unsaturated columns. Experimental and linear combination fit curves are plotted as black and red lines, respectively. The concentrations of solid-phase Fe(II) (D) and As(III) (E) in saturated and unsaturated columns were calculated by combining μXANES and extraction data.

(Figure 5D,E). The results indicated that oxidized species such as Mn(III)/(IV), Fe(III), and As(V) dominated in unsaturated columns, while reduced Mn(II), Fe(II), and As(III) were identified at a higher relative contribution in saturated columns.

Under the unsaturated flow conditions, adsorption maximum positions of Mn, Fe, and As were near 6563, 7134, and 11,875 eV, respectively (Figure 5A–C), indicating the presence of Mn(III)/(IV), Fe(III), As(V), and in the sand columns.[31,32] LCF fitting results of Fe showed a mixture of ferrihydrite and goethite contributed between 61 and 80% along the unsaturated column, except in the sample collected at 6–8 cm depth that contained only 36% of Fe(III) (Figure 5B and Table S4). Additionally, up to 87–93% As(V) was detected along the unsaturated columns (Figure 5C and Table S3). The speciation contribution of Mn, Fe, and As in unsaturated columns is comparable to the solid phase analysis results obtained from a series of household filters in Vietnam.[7,9]

https://doi.org/10.1021/acsestwater.3c00245
ACS EST Water 2024, 4, 33–43

Under the saturated conditions, Mn K-edge XANES spectra of samples taken from the top (0−2 cm) and bottom (5−10 cm) layers showed an adsorption maximum at 6563 eV representing Mn(IV) and indicating a more diffuse distribution than in the unsaturated sample (black arrow, Figure 5D). A shift of the edge position toward lower energy and a concomitant appearance of a shoulder at 6554 eV indicated the presence of Mn(II). Similarly, we also observed an energy shift toward the positions of Fe(II) (7125 eV) from the Fe K-edge XANES spectra of 5−10 cm sand samples (arrow in Figure 5A). LCF fitting results confirmed that Fe(II) was contributing up to 44% to the total Fe pool, equaling 11.6 g/kg (Figure 5D). This finding revealed an expansion of the Fe(III) reduction zone from 6 to 8 cm (in the unsaturated column) to 5−10 cm under saturated conditions. As(III) increased to 15% in the saturated sand column equaling 26−22 mg As(III)/kg which is 10 times more than the amount of As(III) in the unsaturated column.

3.5. MnO_2 Controlling the Fe and As Retention under Semioxic and Anoxic Zones in the Saturated Sand Columns. Under unsaturated conditions, Fe, As, and Mn were primarily present as As(V) adsorbed on Fe(III) (oxyhydr)-oxide and Mn(III)/(IV) oxide minerals. Under saturated flow conditions, we found evidence that microbial Fe(III) and As(V) reduction led to elevated Fe(II) and As(III) in the solid phase that might be oxidized by and associated with Mn(IV) oxides to different extents. The mechanisms of As(III) and Fe(II) oxidation in the presence of Mn(III)(IV) oxides and Fe(III) (oxyhydr)oxide are complex, involving many simultaneously occurring reactions. Based on our observations, the following mechanistic reaction network is proposed to explain Fe-, As-, and Mn-redox speciation in the top and bottom layers of sand columns.

Under saturated conditions, the presence of Mn(II) and As(III) at the top layer (0−2 cm) indicated that Mn(II) and As(III) adsorbed to the surfaces of Fe(III) (oxyhydr)oxide and previously formed Mn oxide minerals. Since the AGW contained high concentrations of bicarbonate, solid-associated Mn(II) also could be present as $MnCO_3$ (rhodochrosite) as previously reported.[33]

The oxidation of As(III) by Mn(IV) oxides in the top layer of the sand column was limited due to (i) the high amount of Fe(II) of 21 mg/L as well as the high Fe/As ratio of 68 in the groundwater so that Fe(II) outcompeted As(III) for adsorption and oxidation on Mn(IV) oxides surface[34,35] and (ii) the formation of Fe(III) (oxyhydr)oxide minerals with adsorbed Mn(II) might cause a surface passivation of Mn oxides thus slowing down As(III) and Fe(II) oxidation.[34,36,37] Even though Mn(IV) oxides might not directly oxidize As(III),[16,34,37−39] these studies confirmed that the presence of Mn oxides maintain high As(V)/As(III) ratios in the solid phase, thus enhancing As immobilization. Additionally, the intermittent feeding of oxygenated water into the sand columns allowed O_2 repenetration into the pore spaces to enhance oxidation processes in the top layers of the SFs.[28,40]

At the bottom layer (5−10 cm), under saturated flow, almost no dissolved oxygen was detected (Figure S3), leading to an increase of Fe(III) reduction (up to 44% of Fe(II) detected in the sand column). The main reason is the microbial reduction of As-bearing Fe(III) (oxyhydr)oxides, as demonstrated in our previous study.[41] The mobilized Fe(II) and desorbed As(V)/(III) likely readsorbed to the remaining Fe(III) (oxyhydr)oxide and Mn(III)/(IV) oxide minerals. While at the SF surface constantly new Fe(III) (oxyhydr)-oxides formed, there was a decrease in available binding sites for Fe(II) and As(III)/(V) on the Fe(III) minerals at the bottom layer. These differences highlight the role of Mn(III)/(IV) oxides on the one hand as a secondary hosting phase and, on the other hand, as oxidant for Fe(II) and As(III). The stronger correlation of Mn with Fe compared to As at the sand surfaces led to the conclusion that Fe(II) adsorbed on Mn oxides was instantaneously oxidized to Fe(III) sequestering As(V) and As(III) into the solid phase. This finding is in line with previous studies on the role of Mn(IV) oxides controlling As mobilization in floodplain soils[16,42] and paddy soils.[43] In addition to the abiotic reduction of Mn(IV) oxides by Fe(II), microbial reduction pathways[44] were probably involved in the elevated Mn(II) concentrations in the effluent in our columns. Nevertheless, bulk XAS for Fe, Mn, and As should be done in the future to obtain better insights into the Fe, Mn, and As binding environment under unsaturated and saturated conditions.

4. CONCLUSIONS

The operation of household SFs for removal of Fe, Mn, and As from water is divided into two phases; it starts with the unsaturated flow when the sand column maintains oxic conditions and is followed by saturated flow when an oxygen gradient is formed along the sand column creating a semioxic (top) and anoxic zone (bottom). By conducting lab- and field-based column experiments, this study showed that groundwater Fe(II) and As(III) were effectively immobilized in sand columns under unsaturated (oxic) and saturated flow conditions. Mn(IV) oxides that formed during the oxic flow acted as a secondary hosting phase and oxidant for Fe(II) and As(III)/(V). Consequently, removal rates of As(III) and Fe(II) were stable at 95 and 99% respectively, while Mn(II) was leached from the sand column, and up to 5.5 mg/L was detected in the effluent. Based on our findings, we therefore provide a few suggestions to improve the performance of household/small-scale SFs applied to remove Mn(II), As(III), and Fe(II) from groundwater as follows. First, intermittent feeding is recommended, rather than continuous flow. The intermittent feeding allows the SFs to completely drain between filtration periods, pulling new air into the pore spaces and reducing the hydraulic conductivity, thus prolonging the time until filter clogging.[28] Second, backwashing as a method to unclogging the filter surface is more beneficial than scrapping off the top sand layer. The scrapping removes a substantial amount of microorganisms accumulated at the top layer, which contribute to Fe, As, and Mn oxidation[9,17,45] while backwashing can preserve better SF's microbial community.[46] Third, the risk of Mn contamination in the effluent should be reduced. In the household filters without backwashing, the top layer of the SF will be removed once the SF is clogged, leading to prolonged saturated conditions in the SFs and consequent Mn remobilization from the filter. Even though Mn(II) is not as toxic as As(III) or As(V), long-term chronic exposure to elevated Mn levels can lead to several adverse health effects.[47−49]

■ ASSOCIATED CONTENT

Supporting Information

The Supporting Information is available free of charge at https://pubs.acs.org/doi/10.1021/acsestwater.3c00245.

https://doi.org/10.1021/acsestwater.3c00245
ACS EST Water 2024, 4, 33−43

Field site description, additional details of column experiments including pictures of the setups, and detailed information on methods used for solid phase analysis (microwave digestion, μ-XANES spectroscopy, visualization of multiple energy μ-XRF maps in SMAK, and As and Fe speciation obtained by LCF) (PDF)

AUTHOR INFORMATION

Corresponding Authors

Anh Van Le − *Geomicrobiology, Department of Geosciences, University of Tuebingen, 72076 Tuebingen, Germany; Department of Environmental Microbiology, Institute for Sanitary Engineering, Water Quality and Solid Waste Management (ISWA), University of Stuttgart, 70569 Stuttgart, Germany*; Phone: +49 711 6685 6374; Email: anh-van.le@uni-tuebingen.de, anh-van.le@iswa.uni-stuttgart.de

Andreas Kappler − *Geomicrobiology, Department of Geosciences, University of Tuebingen, 72076 Tuebingen, Germany; Cluster of Excellence: EXC 2124: Controlling Microbes to Fight Infection, 72076 Tuebingen, Germany*; orcid.org/0000-0002-3558-9500; Phone: +49 7071-29 74992; Email: andreas.kappler@uni-tuebingen.de

Authors

E. Marie Muehe − *Plant Biogeochemistry, Department of Environmental Microbiology, Helmholtz Centre for Environmental Research-UFZ, 04318 Leipzig, Germany; Plant Biogeochemistry, Department of Geosciences, University of Tuebingen, 72076 Tuebingen, Germany*

Sharon Bone − *SLAC National Accelerator Laboratory, Menlo Park, California 94025, United States*; orcid.org/0000-0002-7521-9627

Sören Drabesch − *Geomicrobiology, Department of Geosciences, University of Tuebingen, 72076 Tuebingen, Germany; Plant Biogeochemistry, Department of Environmental Microbiology, Helmholtz Centre for Environmental Research-UFZ, 04318 Leipzig, Germany*

Stefan Fischer − *Tuebingen Structural Microscopy Core Facility, University of Tuebingen, 72076 Tuebingen, Germany*

Complete contact information is available at: https://pubs.acs.org/10.1021/acsestwater.3c00245

Author Contributions

A.V.L contributed to the concept of the study, sampling campaigns, laboratory work, and manuscript writing with support and feedback from A.K and E.M.M. A.K obtained funding and conceptualized the study. Sample preparation, measurement, and data analysis for μXRF were done by S.B, E.M.M. The ICP−MS analysis was conducted by SD. The SEM/EDS was conducted by S.F. The manuscript was revised by all coauthors. CRediT: **Anh Van Le** conceptualization, data curation, formal analysis, investigation, methodology, validation, visualization, writing-original draft, writing-review & editing; **E. Marie Muehe** conceptualization, data curation, formal analysis, methodology, supervision, writing-review & editing; **Sören Drabesch** formal analysis, methodology, writing-review & editing; **Stefan Fischer** data curation, formal analysis, writing-review & editing; **Andreas Kappler** conceptualization, funding acquisition, methodology, project administration, resources, supervision, validation, visualization, writing-review & editing.

Notes

The authors declare no competing financial interest.

ACKNOWLEDGMENTS

This work was funded by the German Research Foundation (DFG, KA1736/41-1). The authors acknowledge infrastructural support by the DFG under Germany's Excellence Strategy, cluster of Excellence EXC2124, project ID 390838134. We also appreciate the Tübingen Structural Microscopy Core Facility (Funded by the Federal Ministry of Education and Research (BMBF) and the Baden-Württemberg Ministry of Science as part of the Excellence Strategy of the German Federal and State Governments) for their support and thank the DFG (INST 37/1027-1 FUGG) for the financial support. We thank Sam Webb at SSRL for beamline support (proposal number 5587). Use of the Stanford Synchrotron Radiation Lightsource, SLAC National Accelerator Laboratory, is supported by the U.S. Department of Energy, Office of Science, Office of Basic Energy Sciences under contract no. DE-AC02-76SF00515. The contents of this publication are solely the responsibility of the authors and do not necessarily represent the official views of NIGMS or NIH. We appreciate the help of our Vietnamese collaborators (P.H. Viet, P. T. K. Trang, V.T. Duyen, The Anh, and P. Tutiyasarn) during the sampling campaigns.

REFERENCES

(1) Freitas, B. L. S.; Terin, U. C.; Fava, N. M. N.; Maciel, P.; Garcia, L.; Medeiros, R.; Oliveira, M.; Fernandez-Ibañez, P.; Byrne, J.; Sabogal-Paz, L. A critical overview of household slow sand filters for water treatment. *Water Res.* **2022**, *208*, 117870.

(2) WHO. *Evaluating Household Water Treatment Options: Health-Based Targets and Microbiological Performance Specifications*; World Health Organization, 2011.

(3) Berg, M.; Tran, H. C.; Nguyen, T. C.; Pham, H. V.; Schertenleib, R.; Giger, W. Arsenic contamination of groundwater and drinking water in Vietnam: A human health threat. *Environ. Sci. Technol.* **2001**, *35* (13), 2621−2626.

(4) Luzi, S.; Berg, M.; Pham, T. K. T.; Pham, H. V.; Schertenleib, R. Household sand filters for arsenic removal; Swiss Fed Inst Environ Sci Technol (EAWAG), Duebendorf, Switz. 2004. http://www.arsenic.eawag.ch/publications (accessed Jan 29, 2019).

(5) Berg, M.; Luzi, S.; Trang, P. T. K.; Viet, P. H.; Giger, W.; Stüben, D. Arsenic removal from groundwater by household sand filters: Comparative field study, model calculations, and health benefits. *Environ. Sci. Technol.* **2006**, *40* (17), 5567−5573.

(6) Nitzsche, K. S.; Lan, V. M.; Trang, P. T. K.; Viet, P. H.; Berg, M.; Voegelin, A.; Planer-Friedrich, B.; Zahoransky, J.; Müller, S. K.; Byrne, J. M.; et al. Arsenic removal from drinking water by a household sand filter in Vietnam- Effect of filter usage practices on arsenic removal efficiency and microbiological water quality. *Sci. Total Environ.* **2015**, *502*, 526−536.

(7) Voegelin, A.; Kaegi, R.; Berg, M.; Nitzsche, K. S.; Kappler, A.; Lan, V. M.; Trang, P. T. K.; Göttlicher, J.; Steininger, R. Solid-phase characterisation of an effective household sand filter for As, Fe and Mn removal from groundwater in Vietnam. *Environ. Chem.* **2014**, *11* (5), 566−578.

(8) Hug, S. J.; Leupin, O. Iron-catalyzed oxidation of Arsenic(III) by oxygen and by hydrogen peroxide: pH-dependent formation of oxidants in the Fenton reaction. *Environ. Sci. Technol.* **2003**, *37* (12), 2734−2742.

(9) Van Le, A.; Straub, D.; Planer-Friedrich, B.; Hug, S. J.; Kleindienst, S.; Kappler, A. Microbial communities contribute to the

elimination of As, Fe, Mn, and NH4+ from groundwater in household sand filters. *Sci. Total Environ.* **2022**, *838*, 156496.
(10) Hansel, C. M. *Manganese in Marine Microbiology*, 1st ed.; Elsevier Ltd.; 2017; Vol. *70*.
(11) Tebo, B. M.; Johnson, H. A.; McCarthy, J. K.; Templeton, A. S. Geomicrobiology of manganese(II) oxidation. *Trends Microbiol.* **2005**, *13* (9), 421−428.
(12) Ross, D. S.; Bartlett, R. J. Evidence for nonmicrobial oxidation of manganese in soil. *Soil Sci.* **1981**, *132* (2), 153−160.
(13) Davies, S. H. R.; Morgan, J. J. Manganese(II) oxidation kinetics on metal oxide surfaces. *J. Colloid Interface Sci.* **1989**, *129* (1), 63−77.
(14) Morgan, J. J. Kinetics of reaction between O2 and Mn (II) species in aqueous solutions. *Geochim. Cosmochim. Acta* **2005**, *69* (1), 35−48.
(15) Petitjean, A.; Forquet, N.; Boutin, C. Oxygen profile and clogging in vertical flow sand filters for on-site wastewater treatment. *J. Environ. Manage.* **2016**, *170*, 15−20.
(16) Ehlert, K.; Mikutta, C.; Kretzschmar, R. Effects of manganese oxide on arsenic reduction and leaching from contaminated floodplain soil. *Environ. Sci. Technol.* **2016**, *50* (17), 9251−9261.
(17) Bai, Y.; Chang, Y.; Liang, J.; Chen, C.; Qu, J. Treatment of groundwater containing Mn(II), Fe(II), As(III) and Sb(III) by bioaugmented quartz-sand filters. *Water Res.* **2016**, *106*, 126−134.
(18) Liu, H.; Xu, R.; Haggblom, M. M.; Zhang, J.; Sun, X.; Gao, P.; Li, J.; Yan, W.; Gao, W.; Gao, P.; et al. Immobile iron-rich particles promote arsenic retention and regulate arsenic biotransformation in treatment wetlands. *Environ. Sci. Technol.* **2022**, *56* (22), 15627−15637.
(19) Webb, S. M.; McNulty, I.; Eyberger, C.; Lai, B. The MicroAnalysis Toolkit: X-ray Fluorescence Image Processing Software. *AIP Conf. Proc.* **2011**, *1365* (1), 196−199.
(20) Ravel, B.; Newville, M. ATHENA, ARTEMIS, HEPHAESTUS: data analysis for X-ray absorption spectroscopy using IFEFFIT. *J. Synchrotron Radiat.* **2005**, *12* (4), 537−541.
(21) Roberts, L. C.; Hug, S. J.; Ruettimann, T.; Billah, M. M.; Khan, A. W.; Rahman, M. T. Arsenic removal with iron (II) and iron (III) in waters with high silicate and phosphate concentrations. *Environ. Sci. Technol.* **2004**, *38* (1), 307−315.
(22) Voegelin, A.; Kaegi, R.; Frommer, J.; Vantelon, D.; Hug, S. J. Effect of phosphate, silicate, and Ca on Fe (III)-precipitates formed in aerated Fe (II)-and As (III)-containing water studied by X-ray absorption spectroscopy. *Geochim. Cosmochim. Acta* **2010**, *74* (1), 164−186.
(23) van Genuchten, C. M.; Gadgil, A. J.; Peña, J. Fe (III) nucleation in the presence of bivalent cations and oxyanions leads to subnanoscale 7 Å polymers. *Environ. Sci. Technol.* **2014**, *48* (20), 11828−11836.
(24) Leupin, O. X.; Hug, S. J. Oxidation and removal of arsenic (III) from aerated groundwater by filtration through sand and zero-valent iron. *Water Res.* **2005**, *39* (9), 1729−1740.
(25) Gülay, A.; Tatari, K.; Musovic, S.; Mateiu, R. V.; Albrechtsen, H. J.; Smets, B. F. Internal porosity of mineral coating supports microbial activity in rapid sand filters for groundwater treatment. *Appl. Environ. Microbiol.* **2014**, *80* (22), 7010−7020.
(26) Han, Y. S.; Kim, S. H.; Jang, J. Y.; Ji, S. Arsenic removal characteristics of natural Mn-Fe binary coating on waste filter sand from a water treatment facility. *Environ. Sci. Pollut. Res.* **2022**, *29* (2), 2136−2145.
(27) Ying, C.; Lanson, B.; Wang, C.; Wang, X.; Yin, H.; Yan, Y.; Tan, W.; Liu, F.; Feng, X. Highly enhanced oxidation of arsenite at the surface of birnessite in the presence of pyrophosphate and the underlying reaction mechanisms. *Water Res.* **2020**, *187*, 116420.
(28) Wielinski, J.; Jimenez-Martinez, J.; Göttlicher, J.; Steininger, R.; Mangold, S.; Hug, S. J.; Berg, M.; Voegelin, A. Spatiotemporal Mineral Phase Evolution and Arsenic Retention in Microfluidic Models of Zerovalent Iron-Based Water Treatment. *Environ. Sci. Technol.* **2022**, *56*, 13696−13708.
(29) Root, R. A.; Fathordoobadi, S.; Alday, F.; Ela, W.; Chorover, J. Microscale speciation of arsenic and iron in ferric-based sorbents subjected to simulated landfill conditions. *Environ. Sci. Technol.* **2013**, *47* (22), 12992−13000.
(30) Hug, S. J.; Leupin, O. X.; Berg, M. Bangladesh and Vietnam: Different groundwater compositions require different approaches to arsenic mitigation. *Environ. Sci. Technol.* **2008**, *42* (17), 6318−6323.
(31) Manning, B. A.; Fendorf, S. E.; Goldberg, S. Surface structures and stability of arsenic(III) on goethite: Spectroscopic evidence for inner-sphere complexes. *Environ. Sci. Technol.* **1998**, *32* (16), 2383−2388.
(32) Tournassat, C.; Charlet, L.; Bosbach, D.; Manceau, A. Arsenic(III) Oxidation by Birnessite and Precipitation of Manganese-(II) Arsenate. *Environ. Sci. Technol.* **2002**, *36* (3), 493−500.
(33) Schaefer, M. V.; Plaganas, M.; Abernathy, M. J.; Aiken, M. L.; Garniwan, A.; Lee, I.; Ying, S. C. Manganese, Arsenic, and Carbonate Interactions in Model Oxic Groundwater Systems. *Environ. Sci. Technol.* **2020**, *54*, 10621−10629.
(34) Wu, Y.; Kukkadapu, R. K.; Livi, K. J. T.; Xu, W.; Li, W.; Sparks, D. L. Iron and Arsenic Speciation during As(III) Oxidation by Manganese Oxides in the Presence of Fe(II): Molecular-Level Characterization Using XAFS, Mossbauer, and TEM Analysis. *ACS Earth Space Chem.* **2018**, *2* (3), 256−268.
(35) Gude, J. C. J.; Rietveld, L. C.; van Halem, D. As(III) oxidation by MnO_2 during groundwater treatment. *Water Res.* **2017**, *111*, 41−51.
(36) Lan, S.; Ying, H.; Wang, X.; Liu, F.; Tan, W.; Huang, Q.; Zhang, J.; Feng, X. Efficient catalytic As (III) oxidation on the surface of ferrihydrite in the presence of aqueous Mn (II). *Water Res.* **2018**, *128*, 92−101.
(37) Ehlert, K.; Mikutta, C.; Kretzschmar, R. Impact of birnessite on arsenic and iron speciation during microbial reduction of arsenic-bearing ferrihydrite. *Environ. Sci. Technol.* **2014**, *48* (19), 11320−11329.
(38) Wu, Y.; Li, W.; Sparks, D. L. The effects of iron (II) on the kinetics of arsenic oxidation and sorption on manganese oxides. *J. Colloid Interface Sci.* **2015**, *457*, 319−328.
(39) Han, X.; Li, Y.-L.; Gu, J.-D. Oxidation of As(III) by MnO2 in the absence and presence of Fe(II) under acidic conditions. *Geochim. Cosmochim. Acta* **2011**, *75* (2), 368−379.
(40) Bretzler, A.; Nikiema, J.; Lalanne, F.; Hoffmann, L.; Biswakarma, J.; Siebenaller, L.; Demange, D.; Schirmer, M.; Hug, S. J. Arsenic removal with zero-valent iron filters in Burkina Faso: Field and laboratory insights. *Sci. Total Environ.* **2020**, *737*, 139466.
(41) Le, A. V.; Muehe, E. M.; Drabesch, S.; Lezama Pacheco, J.; Bayer, T.; Joshi, P.; Kappler, A.; Mansor, M. Environmental Risk of Arsenic Mobilization from Disposed Sand Filter Materials. *Environ. Sci. Technol.* **2022**, *56*, 16822−16830.
(42) Dong, G.; Han, R.; Pan, Y.; Zhang, C.; Liu, Y.; Wang, H.; Ji, X.; Dahlgren, R. A.; Shang, X.; Chen, Z.; et al. Role of MnO2 in controlling iron and arsenic mobilization from illuminated flooded arsenic-enriched soils. *J. Hazard. Mater.* **2021**, *401*, 123362.
(43) Xu, X.; Chen, C.; Wang, P.; Kretzschmar, R.; Zhao, F. J. Control of arsenic mobilization in paddy soils by manganese and iron oxides. *Environ. Pollut.* **2017**, *231*, 37−47.
(44) Cerrato, J. M.; Falkinham, J. O.; Dietrich, A. M.; Knocke, W. R.; McKinney, C. W.; Pruden, A. Manganese-oxidizing and -reducing microorganisms isolated from biofilms in chlorinated drinking water systems. *Water Res.* **2010**, *44* (13), 3935−3945.
(45) Hu, W.; Liang, J.; Ju, F.; Wang, Q.; Liu, R.; Bai, Y.; Liu, H.; Qu, J. Metagenomics Unravels Differential Microbiome Composition and Metabolic Potential in Rapid Sand Filters Purifying Surface Water Versus Groundwater. *Environ. Sci. Technol.* **2020**, *54* (8), 5197−5206.
(46) de Souza, F. H.; Roecker, P. B.; Silveira, D. D.; Sens, M. L.; Campos, L. C. Influence of slow sand filter cleaning process type on filter media biomass: backwashing versus scraping. *Water Res.* **2021**, *189*, 116581.
(47) Ljung, K.; Vahter, M. Time to re-evaluate the guideline value for manganese in drinking water? *Environ. Health Perspect.* **2007**, *115* (11), 1533−1538.

https://doi.org/10.1021/acsestwater.3c00245
ACS EST Water 2024, 4, 33−43

(48) Oulhote, Y.; Mergler, D.; Barbeau, B.; Bellinger, D. C.; Bouffard, T.; Brodeur, M. È.; Saint-Amour, D.; Legrand, M.; Sauvé, S.; Bouchard, M. F. Neurobehavioral function in school-age children exposed to manganese in drinking water. *Environ. Health Perspect.* **2014**, *122* (12), 1343−1350.
(49) Rahman, S. M.; Kippler, M.; Tofail, F.; Bölte, S.; Derakhshani Hamadani, J.; Vahter, M. Manganese in drinking water and cognitive abilities and behavior at 10 years of age: a prospective cohort study. *Environ. Health Perspect.* **2017**, *125* (5), 57003.

https://doi.org/10.1021/acsestwater.3c00245
ACS EST Water 2024, 4, 33−43